Nanoscale Lithography on Monolayer Graphene Using Hydrogenation and Oxidation

Ik-Su Byun,[†] Duhee Yoon,[‡] Jin Sik Choi,[†] Inrok Hwang,[†] Duk Hyun Lee,[†] Mi Jung Lee,[†] Tomoji Kawai,[†,§] Young-Woo Son,[⊥] Quanxi Jia,[†,∥] Hyeonsik Cheong,[‡,*] and Bae Ho Park[†,*]

[†]Division of Quantum Phases & Devices, Department of Physics, Konkuk University, Seoul 143-701, Korea, [‡]Department of Physics, Sogang University, Seoul 121-742, Korea, [§]The Institute of Scientific and Industrial Research, Osaka University, 8-1 Mihogaoka, Ibaraki, Osaka 567-0047, Japan, [⊥]Korea Institute for Advanced Study, Seoul 130-722, Korea, and [∥]Center for Integrated Nanotechnologies, Los Alamos National Laboratory, Los Alamos, New Mexico 87545, United States

ABSTRACT Monolayer graphene is one of the most interesting materials applicable to next-generation electronic devices due to its transport properties. However, realization of graphene devices requires suitable nanoscale lithography as well as a method to open a band gap in monolayer graphene. Nanoscale hydrogenation and oxidation are promising methods to open an energy band gap by modification of surface structures and to fabricate nanostructures such as graphene nanoribbons (GNRs). Until now it has been difficult to fabricate nanoscale devices consisting of both hydrogenated and oxidized graphene because the hydrogenation of graphene requires a complicated process composed of large-scale chemical modification, nanoscale patterning, and etching. We report on nanoscale hydrogenation and oxidation of graphene under normal atmospheric conditions and at room temperature without etching, wet process, or even any gas treatment by controlling just an external bias through atomic force microscope lithography. Both the lithographically defined nanoscale hydrogenation and oxidation have been confirmed by micro-Raman spectroscopy measurements. Patterned hydrogenated and oxidized graphene show insulating behaviors, and their friction values are several times larger than those of graphene. These differences can be used for fabricating electronic or electromechanical devices based on graphene.

KEYWORDS: graphene hydrogenation · graphene oxidation · nanoscale lithography · atomic force microscope · Raman spectroscopy

Nanoelectronics based on monolayer graphene has attracted a great deal of attention in recent years due to graphene's high carrier mobilities.[1−6] Since monolayer graphene is a zero-gap semimetal with two linear bands crossing at the Dirac point, much effort has been devoted to creating a considerable energy gap in graphene-based materials for device applications.[2,3,7] For that purpose, chemical modifications such as hydrogenation and oxidation have been routinely used and can realize an energy gap with different atomic structures.[8]

In previous attempts, hydrogen plasma was used to modulate the electronic properties of individual graphene flakes, turning them into so-called graphane insulators.[5,9] Oxygen treatment was also applied to create graphene islands.[4] Since these methods induce chemical modification over a large area, special patterning and etching methods are required to apply such hydrogenation and oxidation for graphene-based nanoelectronics. In addition, those methods require special conditions, such as high temperatures, low pressures, high-voltage electric fields, and high purity gas sources.

If controlled nanoscale hydrogenation and oxidation become feasible, one can modify electronic structures of graphene on the nanoscale and, furthermore, define ultranarrow graphene nanoribbon (GNR) circuits right on top of pristine graphene. In addition, the two-dimensional superlattice structures that have theoretically been proposed to open a band gap in monolayer graphene would become a possibility.[10−12] Therefore, nanoscale hydrogenation and oxidation can lead to facile fabrication of nanoelectronic devices based on graphene.

Nanoscale patterning has been explored in various materials using atomic force microscope (AFM) lithography.[13] In the past few years, AFM lithography has also been used for the fabrication of patterns on graphene[14−18] or graphene oxide (GO).[19−21] However, locally controlled nanoscale hydrogenation of monolayer graphene has not been reported yet. Moreover, systematic studies of oxidation in the AFM lithography methods, especially by Raman spectroscopy, have been lacking. Since hydrogenated and oxidized graphene should show different electronic behaviors, having the capability to control both hydrogenation and oxidation in nanoscale will be very useful for designing a wide range of graphene devices.

* Address correspondence to hcheong@sogang.ac.kr, baehpark@konkuk.ac.kr.

Received for review May 2, 2011 and accepted July 21, 2011.

Published online July 21, 2011
10.1021/nn201601m

In this report, nanoscale hydrogenated and oxidized graphenes were formed on mechanically exfoliated graphene supported on silicon substrates at ambient temperature and pressure, using AFM lithography. Hydrogenation and oxidation were confirmed by micro-Raman spectroscopy. Both hydrogenated and oxidized graphene were highly insulating compared to pristine graphene, while also showing friction values 3 times and 8 times larger, respectively. This opens up the possibility of integrating graphene with oxidized and/or hydrogenated graphene for electronic or electromechanical devices.

RESULTS AND DISCUSSION

Figure 1a shows a schematic diagram of the AFM lithography setup. When a negative dc bias voltage is applied to a graphene sample using AFM (negative lithography), positive hydrogen ions (H^+) which are dissociated electrically from water molecules (H_2O) can be adsorbed on the graphene surface which acts as a cathode. Since it is expected that hydrogen ions are reduced at the graphene surface and readily form hydrogen atoms, the graphene surface can be hydrogenated by the reactive hydrogen atoms and some remaining positive hydrogen ions. Furthermore, a density functional theory calculation[22] indicates that hydrogenation of graphene can occur even with gaseous hydrogen created by chemical reaction ($2H^+ + 2e^- \rightarrow H_2$) during AFM lithography if a negative perpendicular electric field is applied to reduce the energy barrier for hydrogen atom dissociative adsorption on graphene. After hydrogenation on graphene, the remaining oxyanions (OH^-) can contribute to the formation of oxide on the AFM tip.

When a positive dc bias voltage is applied to a graphene sample using AFM (positive lithography), it is expected that oxides grow on graphene which acts as an anode. There is a threshold voltage at which the anodic oxidation starts. A high electric field ($E > 10^7$ V/m) can decompose water molecules adsorbed on graphene into ions (*e.g.*, H^+, OH^-, and O^{2-}). Negatively charged oxygen-containing radicals (*e.g.*, OH^- and O^{2-}) can be attracted to the anode and contribute to the formation of surface oxides and also to the successive growth of the oxide underneath.[23]

We have fabricated four different areas (3 μm $\times$ 3 μm) by negative and positive AFM lithography in order to study differences between the areas patterned using dc biases with opposite polarity. We can easily distinguish the areas formed by positive AFM lithography using optical microscopy since they are optically indistinguishable from the 300-nm-thick SiO_2, while pristine graphene shows a slight contrast, as shown in Figure 1b. Figure 1c shows a topographic AFM image including blue and red rectangular areas on mono- (top) and bilayer (bottom) graphene samples at a writing voltage (-7 V and $+7$ V) and a writing speed of 0.1 μm/s formed by negative and positive AFM lithography, respectively. The areas formed by positive AFM lithography (denoted by two red rectangles) have a height of 3 nm and are easily distinguished by optical microscopy. In contrast, it is more difficult to observe areas formed by negative AFM lithography (two blue rectangles). Both types of patterned surfaces are as smooth as those of graphene samples or silicon oxide substrates (Figure S1, Supporting Information).

Micro-Raman spectroscopy has been used to characterize the blue and red rectangular areas formed by AFM lithography on mono- and bilayer graphene (Figures 1d and 1e, respectively). Since the size of rectangular areas is larger than the laser spot size (0.7 μm), we can take clear Raman spectroscopy data neglecting any contribution to the Raman spectra from pristine graphene outside the well-defined rectangular areas.

The main features in the Raman spectra of carbon based materials are the D and G bands that lie at around 1350 and 1580 cm^{-1}, respectively.[5,24] Calculations of the Raman response indicate that the D band is induced by local basal plane derivatization with sp^3 distortion. The G band corresponds to optical E_{2g} phonons at the Brillouin zone center, whereas the D band is caused by breathing-like modes and requires a defect for its activation *via* an intervalley double-resonance Raman process.[24]

Raman spectra taken from pristine mono- and bilayer graphenes before AFM lithography are shown in Figure 1 panels d and e, respectively, showing two intense bands, the G band at 1580 cm^{-1} and the 2D band at 2700 cm^{-1} which are characteristics of pristine mono- and bilayer graphenes.[25,26] The 2D band is ascribed to the Stokes−Stokes double resonant scattering involving two iTO phonons near the K point of the Brillouin zone. Because of the resonant nature, the 2D bands of pristine mono- and bilayer graphene reflect the band structure of graphene and are very strong.[27] The Raman spectra show no detectable defect-related Raman D band ($\sim$1350 cm^{-1}), indicating that both the mono- and bilayer graphenes contain initially very low density of defects.

As shown in Figure 1d,e (blue lines), negative AFM lithography results in the appearance of the sharp D′ and D bands and the onset of a combination mode (D + D′) around 2950 cm^{-1}. The 2D bandwidth is slightly broadened and its relative height to the G band decreases. The *D′* band located at $\sim$1620 cm^{-1} occurs *via* an intravalley double-resonance process in the presence of defects.[25] The (D + D′) band also requires a defect for its activation because it is a combination of two phonons with different momenta.[5] The D band for the region patterned by negative AFM lithography on monolayer graphene is sharper than that in disordered or nanostructured carbon-based materials.[26] We attribute the activation of this sharp D band to

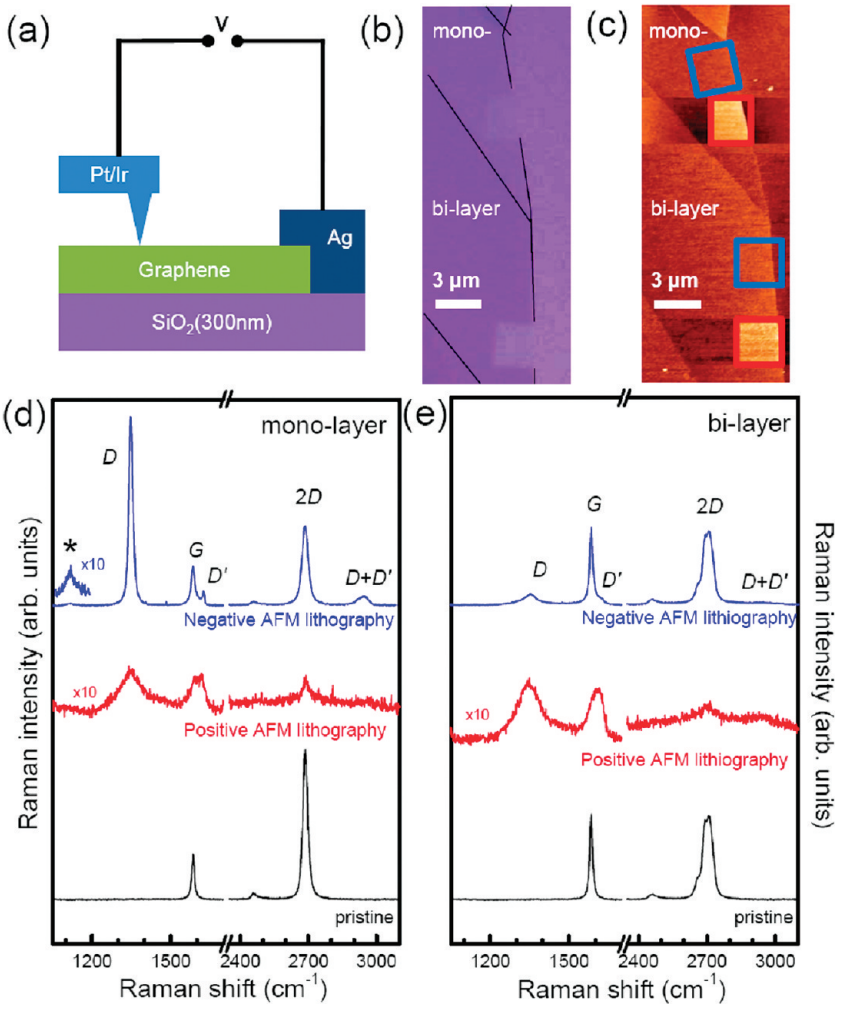

Figure 1. Patterns formed using negative and positive AFM lithography on mono- and bilayer graphene: (a) schematic diagram of the AFM lithography setup; (b) optical microscope image; (c) topographic AFM image; and Raman spectra of (d) mono- and (e) bilayer graphene. The black lines in panel b indicate boundaries between SiO_2, monolayer graphene, and bilayer graphene. The blue and red rectangular regions shown in panel c are areas formed by negative and positive AFM lithography, respectively.

breaking of the translational symmetry of C−C sp^2 bonds after negative AFM lithography. We also detected a small ∗ band (1116 cm^{-1}) from patterned monolayer graphene. This band is often found in free-standing hydrogenated monolayer graphene,[5] as reported in the supporting information of ref 5, and is a strong indication of hydrogenation. In the case of bilayer graphene, after performing negative AFM lithography, a much smaller intensity of D band is observed compared with that of monolayer graphene. Monolayer graphenes, either free-standing or supported on SiO_2 substrates, have significant ripples[9] while such ripples were found to decrease with increasing thickness of the graphene samples.[9] The hydrogenation is expected to occur preferentially on top of ripples promoting sp^3 hybridization in sp^2-hybridized carbons in the presence of hydrogen radicals.[5,9] Therefore, measurements through either optical microscopy or topographic AFM images cannot distinguish the hydrogenated area from the pristine owing to the low coverage of hydrogenation on top of the ripples while the Raman spectroscopy can (Figure 1b,c). These phenomena also explain why monolayer graphene is more reactive than bilayer graphene.

For the regions patterned using positive AFM lithography in both mono- and bilayer graphenes, the Raman spectra (red lines) are dramatically modified from those of pristine graphene. They show three main bands of D, G, and 2D. The disorder-induced D band, which is not detectable in our pristine graphene, can be detected although it has a low intensity. We find that the intensity of the 2D band is reduced for the region patterned by positive AFM lithography, implying a significantly modified atomic structure. The G band is broadened and shifts to a significantly higher frequency (1607 cm^{-1}) compared to 1583 cm^{-1} of the pristine graphene. All these characteristics in the Raman data for the regions patterned by positive AFM lithography are similar to those found in graphene oxidized by thermal oxidation or modified Hummer method.[4,25,28,29]

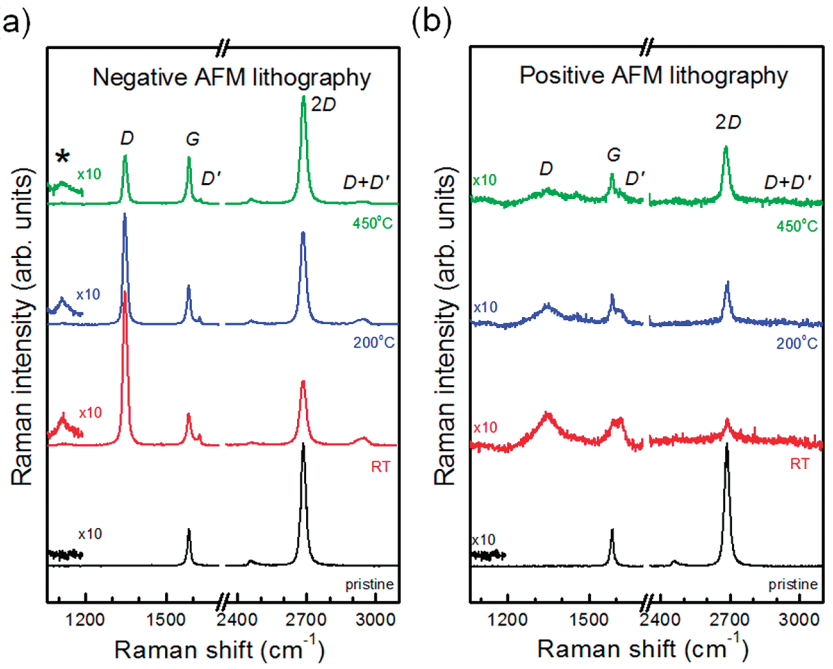

Figure 2. Raman spectra from the treated areas on monolayer graphene using (a) negative and (b) positive AFM lithography before and after vacuum annealing for 2 h at 200 and 450 °C in 5 mTorr of Ar atmosphere.

During thermal annealing, graphene samples patterned by negative or positive AFM lithography are expected to undergo structural changes due to the loss of hydrogen or oxygen, respectively. The carbon atoms in the basal plane may also rearrange during annealing owing to the available thermal energy.[29] Such structural changes can be monitored by micro-Raman spectroscopy measurements taken after each annealing step in Ar gas at 5 mTorr, as shown in Figure 2.

The reduction of the D band intensity due to annealing is more pronounced in the area formed on monolayer graphene by negative AFM lithography (Figure 2a). The intensity of the small $*$ band (1116 cm^{-1}) also decreases after annealing. On the other hand, the intensities of the G and 2D bands increase with annealing temperature. This corresponds to the weaker bonding strength between carbon and hydrogen in the hydrogenated graphene than that between carbon and oxygen in graphene oxide, leading to an easier removal of hydrogen atoms by annealing. These results are in good agreement with previous reports for plasma induced hydrogenation.[5,9]

Figure 2b shows a shift of the *G* band toward lower frequency when the area formed by positive AFM lithography is annealed at an elevated temperature, agreeing with observations in the previous GO experiments.[29] As the annealing temperature increases, the intensities of the D, D′, and D + D′ bands decrease, whereas those of the G and 2D bands increase. This is an indication of annealing-induced recovery of the sp^2 honeycomb structure of graphene as the oxygen atoms are removed from the patterned area.[9] Therefore, we can confirm that the areas written on mono- and bilayer graphenes by negative and positive AFM lithography are hydrogenated and oxidized, respectively.

After confirming hydrogenation and oxidation of graphene by AFM lithography through Raman spectroscopy, first we examined the dependence of the patterned line width on the writing voltage at a constant writing speed of 0.1 μm/s (Figure 3a) and on the writing speed at a constant writing voltage of -7 V (Figure 3b). The patterns are written on a monolayer graphene using negative AFM lithography at a constant loading force of 1 nN and relative humidity (RH) of 33%. As mentioned earlier, because it was difficult to distinguish regions patterned by negative AFM lithography by topographic AFM (right), we used frictional force microscope (FFM) images (left) due to higher friction value of hydrogenated graphene from pristine regions. From the image in Figure 3a we can infer that the experimental threshold voltage for the hydrogenation on monolayer graphene using negative AFM lithography is -6 V at the writing speed of 0.1 μm/s. The line width by negative AFM lithography increases with the tip−sample voltage. The width of the lines formed at -6 and -10 V was 107 and 125 nm, respectively. As shown in Figure 3a, the FFM image becomes less clear and we could no longer measure the width at less than -5 V at the writing speed of 0.1 μm/s. Similarly, the line width decreased with increasing scan speed from 0.1 to 1.0 μm/s as described in Figure 3b; however, it was difficult to measure the exact width and increase for hydrogenation.

Next we considered the dependence of the pattern width in positive AFM lithography and demonstrated

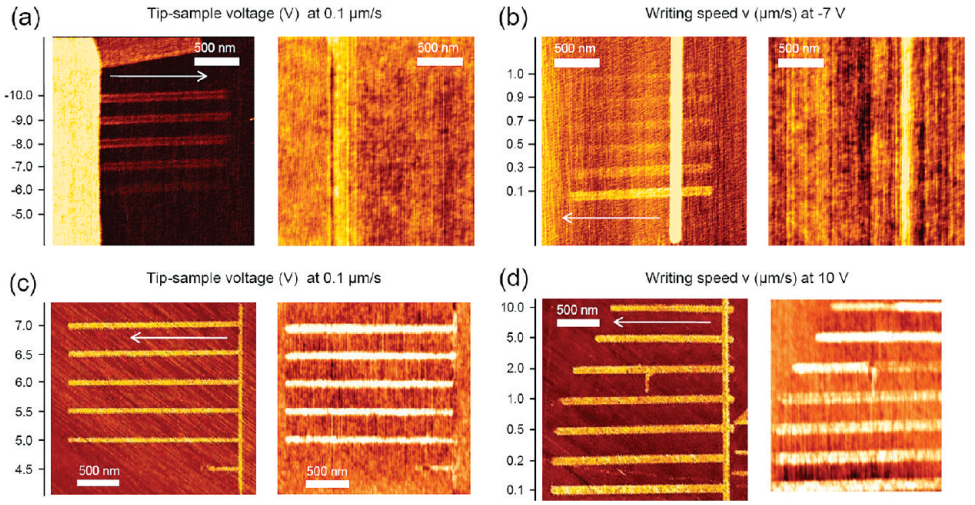

Figure 3. Images of lines written on monolayer graphene using AFM: frictional force microscope (FFM) images (left) and topographic images (right) of lines written under various (a) negative and (c) positive dc bias at a constant writing speed of 0.1 μm/s, and lines written under various writing speed at a constant dc bias of (b) −7 and (d) 10 V. Loading force and RH were kept at constant values of 1 nN and negative (positive) 33% (20%), respectively, during writing. White arrows indicate the scan directions during AFM lithography.

that one can control the width of oxidized line from 45 to 82 nm by changing the bias voltage and scan speed. Here we change writing voltages from 4.5 to 10 V at a constant writing speed of 0.1 μm/s (Figure 3c). In other cases, the writing speeds are varied from 0.1 to 1.0 μm/s at a constant writing voltage of 10 V (Figure 3d). We use a constant loading force of 1 nN and RH of 20%. We chose a lower RH of 20% in order to minimize the line width which is significant for AFM-based nanolithography.[30,31] When a 4.5 V bias is applied to a monolayer graphene sample with respect to the AFM tip at a writing speed of 0.1 μm/s, the formation of a barely distinguishable line begins, as shown in Figure 3c, although the formation of the line does not continue along the whole length of writing. We infer that the experimental threshold voltage for the oxidation on monolayer graphene using positive AFM lithography is 4.5 V at the writing speed of 0.1 μm/s. As with negative AFM lithography the line width by positive AFM lithography increases with the tip−sample voltage. The width of the lines formed at 5 and 7 V was 45 and 55 nm, respectively. When the writing speed is increased gradually, the line width decreases again, as shown in Figure 3d. The width of the lines formed at writing speeds of 0.1 and 10 μm/s with a fixed writing voltage of 10 V is 82 and 61 nm, respectively. The widths of the oxidized regions are much easier to measure compared to the hydrogenated regions mentioned earlier. The topographic AFM images of Figure 3c,d show that bump structures with a height of around 2 nm are formed on monolayer graphene by positive AFM lithography. Our result shows that nanoscale patterns can be written with a high resolution on monolayer graphene using both negative and positive AFM lithography with a bias less than 10 V.

Besides the bias voltage and scan speed, humidity is also a very important factor for nanoscale patterning of graphene by AFM lithography. At low humidity, it is impossible to write a pattern using AFM lithography starting from the center area of a monolayer graphene sample since the C−C bonds in a graphene sheet are too strong to be broken directly.[14] Humidity is also known to have a dramatic effect on friction of the hydrophilic hydrogenated graphene surface *via* formation of hydrogen bonds leading to considerably increased friction compared to nominally dry conditions.[32] AFM lithography can change the surface from hydrophobic to hydrophilic states by hydrogenation resulting in a change of the friction force of monolayer graphene (Figure S2, Supporting Information). Therefore it is practical to start writing patterns using AFM lithography from a point already patterned or a graphene edge due to easier formation of water-meniscus between the AFM tip and the point underneath it. In fact, nanoscale AFM lithography is readily initiated from the edges on monolayer graphene even at low relative humidity (and thus finer line widths), and then it can be extended from the edge to the center by scanning.

Finally, for the applicability of AFM lithography toward graphene devices, an electrically isolated conductive island has been demonstrated by fabricating rectangular-shaped insulating hydrogenated or oxidized lines on monolayer graphene. Figure 4a shows FFM (left) and conducting AFM (C-AFM) (right) images of areas patterned using blue dashed hydrogenated (−10 V, 0.1 μm/s) or red dashed oxidized (+7 V, 0.1 μm/s) lines. The hydrogenated lines were fabricated with sequentially increased loading force, 1 → 2 → 4 nN, for high coverage of hydrogen atoms on graphene. During the C-AFM measurement, 0.1 V dc bias

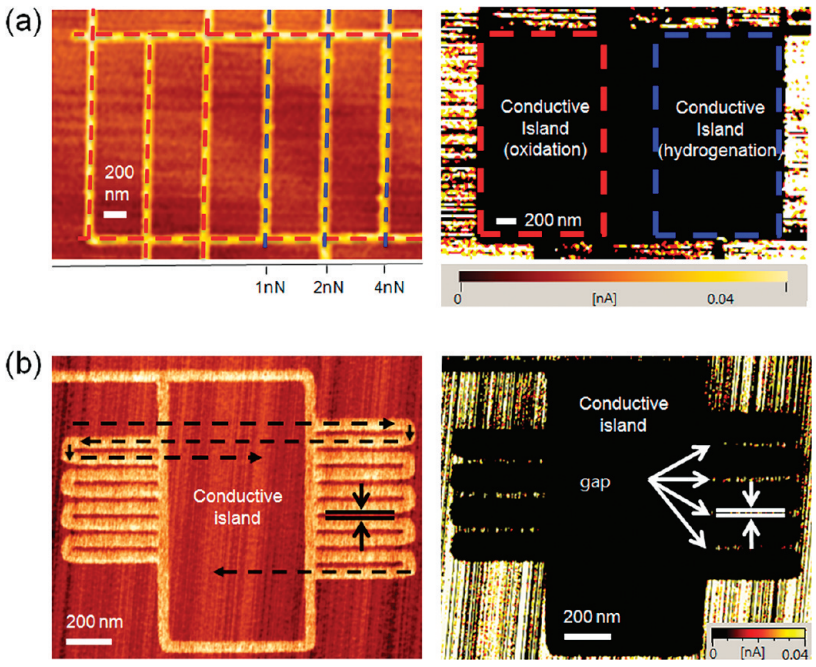

Figure 4. Nanoscale images of electrically isolated regions formed on monolayer graphene using negative and positive AFM lithography: (a, left) FFM and (a, right) C-AFM images of areas surrounded by hydrogenated or oxidized lines; (b, left) FFM and (b, right) C-AFM images of the regions formed by oxidized lines with the square pattern initiated from the top-left edge and then scanning through black dashed lines. Blue and red dashed lines in image a denote hydrogenated and oxidized lines, respectively. Panel b shows that sub-20 nm conducting gaps are formed between neighboring insulating oxidized graphene lines.

was applied between a C-AFM tip and a ground electrode located outside the conductive island. The current value less than 5 pA at the areas surrounded by the hydrogenated or oxidized lines confirms that hydrogenated or oxidized graphene is highly insulating.

After making a conductive island surrounded by oxidized lines, we have drawn several horizontal lines as indicated by the black dashed lines in Figure 4b. We cannot form lines inside the conductive island using positive AFM lithography whose ground electrode is located outside the island. Thus, we can conclude that the conductive islands are electrically isolated from the surrounding area by oxidized or hydrogenated graphene regions. The insulating behaviors of hydrogenated and oxidized graphene are in good agreement with previous reports for hydrogenated[5] and oxidized graphene[20,29] formed by other methods requiring extreme conditions.

Using AFM lithography, we have also successfully fabricated electrically isolated island structures on tri- and tetralayer graphene samples whose bottom-most layers are electrically connected to ground electrodes (Figure S3, Supporting Information). Isolated properties of multiple graphene sheets may result from propagation of oxidation perpendicular to the surface, similarly to the case of highly oriented pyrolytic graphite (HOPG) which has been previously reported.[33] Since we can control the gap between neighboring insulating patterned lines down to 10 nm, as shown in Figure 4b and Supporting Information, Figure S4, AFM lithography can be a promising method for fabricating devices based on graphene.

Although AFM lithography methods have limited throughput, the manufacture of graphene quantum devices could be achieved by using arrays of probe tips.[34] Independently addressed probe tips could alternately read or write nanostructures on a surface and large arrays could address wafer-scale areas at high speed. This method may be widely used to fabricate quantum devices with high throughput. Moreover, controllable local frictions may make oxidized and hydrogenated graphene candidates for lubricants in microscale or nanoscale electromechanical devices to control the interaction at the contact area between materials.

SUMMARY

We developed a facile method to achieve nanoscale hydrogenation and oxidation of graphene under normal atmospheric conditions and at room temperature using AFM lithography. By changing the polarity of applied voltage between graphene and a conductive AFM tip, we could control hydrogenation and oxidation on the nanoscale. The lithographically defined nanoscale hydrogenated and oxidized graphene were confirmed by micro-Raman spectroscopy measurements. Both are insulating as well as have several times larger friction values than those of pristine graphene. We also demonstrated that the pattern widths can be

controlled by changing the scan speed and voltage of the conductive AFM tip. The methods here could easily extend to fabricate conductive and hydrophobic GNR with dimensions down to sub-10 nm width surrounded by insulating and hydrophilic patterned lines on monolayer graphene.

EXPERIMENTAL SECTION

Graphene layers were prepared by the standard exfoliation method as introduced in other papers[4,5] from natural graphite supported on a thermally grown 300-nm-thick SiO_2 on a Si substrate. The graphene layers were identified by their color contrast under an optical microscope followed by thickness measurements using AFM and Raman spectroscopy. The Raman spectra were obtained using a micro-Raman system using the 514.5-nm line of an Ar ion laser as the excitation source. Other experimental details have been previously reported.[25]

The nanoscale lithography was performed at normal temperature and pressure by a contact mode AFM (Nanofocus n-Tracer AFM system and SEIKO SPI300HV). A Si cantilever with a Pt/Ir coated conductive tip (Point Probe series, NANOSENSORS) was used to apply local dc bias voltage between a graphene sample and the conductive AFM tip. The spring constant and resonance frequency were set to 0.2 N/m and 13 kHz, respectively. The RH was maintained at ~20% and at ~33%. To avoid surface contamination from resist residues, electrode contact pads were formed using colloidal silver paste (TED PELLA), instead of the conventional electron beam lithography technique.[14−18]

Acknowledgment. This work was supported by the following National Research Foundation of Korea (NRF) grants funded by the Ministry of Education, Science and Technology (MEST): Basic Science Research Program (Grant No. KRF-2008-314-C00111), National Research Laboratory (NRL) Program (2008-0060004), World Class University (WCU) Program (Grant No. R31-2008-000-10057-0), Quantum Metamaterials Research Center (Grant No. R11-2008-053-03002-0), Nano R&D program (2008-2003670), and Midcareer Researcher Program (2011-0017605). I.-S.B. was supported by Hi Seoul Science / Humanities Fellowship from Seoul Scholarship Foundation.

Supporting Information Available: (1) Surface roughness of patterned areas on monolayer graphene; (2) friction of hydrogenated and oxidized monolayer graphene; (3) electrical isolation using oxidation on tri- and tetralayer graphene; (4) narrow graphene gap between patterned regions. This material is available free of charge *via* the Internet at http://pubs.acs.org.

REFERENCES AND NOTES

1. Balog, R.; Jørgensen, B.; Nilsson, L.; Andersen, M.; Rienks, E.; Bianchi, M.; Fanetti, M.; Lægsgaard, E.; Baraldi, A.; Lizzit, S.; *et al*. Bandgap Opening in Graphene Induced by Patterned Hydrogen Adsorption. *Nat. Mater.* **2010**, *9*, 315–319.
2. Son, Y.-W.; Cohen, M. L.; Louie, S. G. Energy Gaps in Graphene Nanoribbons. *Phys. Rev. Lett.* **2006**, *97*, 216803.
3. Rotenberg, E.; Bostwick, A.; Ohta, T.; McChesney, J. L.; Seyller, T.; Horn, K. Origin of the Energy Bandgap in Epitaxial Graphene. *Nat. Mater.* **2008**, *7*, 258–259.
4. Liu, L.; Ryu, S.; Tomasik, M. R.; Stolyarova, E.; Jung, N.; Hybertsen, M. S.; Steigerwald, M. L.; Brus, L. E.; Flynn, G. W. Graphene Oxidation: Thickness-Dependent Etching and Strong Chemical Doping. *Nano Lett.* **2008**, *8*, 1965–1970.
5. Elias, D. C.; Nair, R. R.; Mohiuddin, T. M. G.; Morozov, S. V.; Blake, P.; Halsall, M. P.; Ferrari, A. C.; Boukhvalov, D. W.; Katsnelson, M. I.; Geim, A. K.; *et al*. Control of Graphene's Properties by Reversible Hydrogenation: Evidence for Graphane. *Science* **2009**, *323*, 610–613.
6. Geim, A. K.; Novoselov, K. S. The Rise of Graphene. *Nat. Mater.* **2007**, *6*, 183–191.
7. Pereira, V. M.; Castro Neto, A. H.; Peres, N. M. R. Tight-Binding Approach to Uniaxial Strain in Graphene. *Phys. Rev. B* **2009**, *80*, 045401.
8. Sofo, J. O.; Chaudhari, A. S.; Barber, G. D. Graphane: A Two-Dimensional Hydrocarbon. *Phys. Rev. B* **2007**, *75*, 153401.
9. Ryu, S.; Han, M. Y.; Maultzsch, J.; Heinz, T. F.; Kim, P.; Steigerwald, M. L.; Brus, L. E. Reversible Basal Plane Hydrogenation of Graphene. *Nano Lett.* **2008**, *8*, 4597–4602.
10. Li, X.; Wang, X.; Zhang, L.; Lee, S.; Dai, H. Chemically Derived, Ultrasmooth Graphene Nanoribbon Semiconductors. *Science* **2008**, *319*, 1229–1232.
11. Han, M. Y.; Ozyilmaz, B.; Zhang, Y.; Kim, P. Energy Band-Gap Engineering of Graphene Nanoribbons. *Phys. Rev. Lett.* **2007**, *98*, 206805.
12. Park, C.-H.; Yang, L.; Son, Y.-W.; Cohen, M. L.; Louie, S. G. Anisotropic Behaviours of Massless Dirac Fermions in Graphene under Periodic Potentials. *Nat. Phys.* **2008**, *4*, 213–217.
13. Martínez, R. V.; Losilla, N. S.; Martinez, J.; Huttel, Y.; Garcia, R. Patterning Polymeric Structures with 2 nm Resolution at 3 nm Half Pitch in Ambient Conditions. *Nano Lett.* **2007**, *7*, 1846–1850.
14. Giesbers, A. J. M.; Zeitler, U.; Neubeck, S.; Freitag, F.; Novoselov, K. S.; Maan, J. C. Nanolithography and Manipulation of Graphene Using an Atomic Force Microscope. *Solid State Commun.* **2008**, *147*, 366–369.
15. Weng, L.; Zhang, L.; Chen, L.; Chen, Y. P.; Rokhinson, L. P. Atomic Force Microscope Local Oxidation Nanolithography of Graphene. *Appl. Phys. Lett.* **2008**, *93*, 093107.
16. Masubuchi, S.; Ono, M.; Yoshida, K.; Hirakawa, K.; Machida, T. Fabrication of Graphene Nanoribbon by Local Anodic Oxidation Lithography Using Atomic Force Microscope. *Appl. Phys. Lett.* **2009**, *94*, 082107.
17. Puddy, R. K.; Scard, P. H.; Tyndall, D.; Connolly, M. R.; Smith, C. G.; Jones, G. A. C.; Lombardo, A.; Ferrari, A. C.; Buitelaar, M. R. Atomic Force Microscope Nanolithography of Graphene: Cuts, Pseudocuts, and Tip Current Measurements. *Appl. Phys. Lett.* **2011**, *98*, 133120.
18. Neubeck, S.; Ponomarenko, L. A.; Freitag, F.; Giesbers, A. J. M.; Zeitler, U.; Morozov, S. V.; Blake, P.; Geim, A. K.; Novoselov, K. S. From One Electron to One Hole: Quasiparticle Counting in Graphene Quantum Dots Determined by Electrochemical and Plasma Etching. *Small* **2010**, *6*), 1469–1473.
19. Lu, G.; Zhou, X.; Li, Hai.; Yin, Z.; Li, B.; Huang, L.; Boey, F.; Zhang, H. Nanolithography of Single-Layer Graphene Oxide Films by Atomic Force Microscopy. *Langmuir* **2010**, *26*, 6164–6166.
20. Mativetsky, J. M.; Treossi, E.; Orgiu, E.; Melucci, M.; Veronese, G. P.; Samorí, P.; Palermo, V. Local Current Mapping and Patterning of Reduced Graphene Oxide. *J. Am. Chem. Soc.* **2010**, *132*, 14130–14136.
21. Wei, Z. Q.; Wang, D. B.; Kim, S.; Kim, S. Y.; Hu, Y. K.; Yakes, M. K.; Laracuente, A. R.; Dai, Z. T.; Marder, S. R.; Berger, C.; *et al*. Nanoscale Tunable Reduction of Graphene Oxide for Graphene Electronics. *Science* **2010**, *328*, 1373–1376.
22. Ao, Z. M.; Peeters, F. M. Electric Field: a Catalyst for Hydrogenation of Graphene. *Appl. Phys. Lett.* **2010**, *96*, 253106.
23. Červenka, J.; Kalousek, M.; Bartošík, M.; Škoda, D.; Tomanec, O.; Šikola, T. Fabrication of Nanostructures on Si(100) and GaAs(100) by Local Anodic Oxidation. *Appl. Surf. Sci.* **2006**, *253*, 2373–2378.
24. Kudin, K. N.; Ozbas, B.; Schniepp, H. C.; Prud'homme, R. K.; Aksay, I. A.; Car, R. Raman Spectra of Graphite Oxide and Functionalized Graphene Sheets. *Nano Lett.* **2008**, *8*, 36–41.
25. Yoon, D.; Moon, H.; Cheong, H.; Choi, J. S.; Choi, J. A.; Park, B. H. Variations in the Raman Spectrum as a Function of the Number of Graphene Layers. *J. Korean Phys. Soc.* **2009**, *55*, 1299–1303.

26. Ferrari, A. C.; Robertson, J. Interpretation of Raman Spectra of Disordered and Amorphous Carbon. *Phys. Rev. B* **2000**, *61*, 14095.
27. Ferrari, A. C.; Meyer, J. C.; Scardaci, V.; Casiraghi, C.; Lazzeri, M.; Mauri, F.; Piscanec, P.; Jiang, D.; Novoselov, K. S.; Roth, S.; Geim, A. K. Raman Spectrum of Graphene and Graphene Layers. *Phys. Rev. Lett.* **2006**, *97*, 187401.
28. Yang, D.; Velamakanni, A.; Bozoklu, G.; Park, S.; Piner, R. D.; Stankovich, S.; Jung, I.; Field, D. A.; Ventrice, J. C. A.; Ruoff, R. S. Chemical Analysis of Graphene Oxide Films after Heat and Chemical Treatments by X-ray Photoelectron and Micro-Raman Spectroscopy. *Carbon* **2009**, *47*, 145–152.
29. Mattevi, C.; Eda, G.; Agnoli, S.; Miller, S.; Mkhoyan, K. A.; Celik, O.; Mastrogiovanni, D.; Granozzi, G.; Garfunkel, E.; Chhowalla, M. Evolution of Electrical, Chemical, and Structural Properties of Transparent and Conducting Chemically Derived Graphene Thin Films. *Adv. Funct. Mater.* **2009**, *19*, 2577–2583.
30. Johannes, M. S.; Cole, D. G.; Clark, R. L. Velocity Controlled Anodization Nanolithography with an Atomic Force Microscope Using Faradaic Current Feedback. *Appl. Phys. Lett.* **2007**, *90*, 103106.
31. Avouris, P.; Hertel, T.; Martel, R. Atomic Force Microscope Tip-Induced Local Oxidation of Silicon: Kinetics, Mechanism, and Nanofabrication. *Appl. Phys. Lett.* **1997**, *71*, 285.
32. Liu, Y.; Szlufarska, I. Effect of Trace Moisture on Friction. *Appl. Phys. Lett.* **2010**, *96*, 101902.
33. Neubeck, S.; Freitag, F.; Yang, R.; Novoselov, K. S. Scanning Probe Lithography on Graphene. *Phys. Status Solidi B* **2010**, *247*, 2904–2908.
34. Minne, S. C.; Adams, J. D.; Yaralioglu, G.; Manalis, S. R.; Atalar, A.; Quate, C. F. Centimeter Scale Atomic Force Microscope Imaging and Lithography. *Appl. Phys. Lett.* **1998**, *73*, 1742.